PHYSICAL REVIEW A VOLUME 34, NUMBER 4 OCTOBER 1986

Theoretical study of electronic autoionization in CO: Vibrationally resolved results between 17 and 18.3 eV

B. Leyh
Département de Chimie générale, Université de Liège, B-4000 Sart-Tilman par Liège 1, Belgium

G. Raşeev
Laboratoire de Photophysique Moléculaire, Bâtiment 213, Université de Paris-Sud, F-91405 Orsay, France and Département de Chimie générale, Université de Liège, B-4000 Sart-Tilman par Liège 1, Belgium

(Received 13 December 1985)

We have theoretically studied the electronic autoionization between 17 and 18.3 eV of the Rydberg series converging to the $B\,^2\Sigma^+$ state of CO^+ (R_B series). We have obtained the partial and vibrationally resolved differential and total photoionization cross sections by combining *ab initio* electronic quantities with a variant of the two-step multichannel quantum-defect theory (MQDT). The formalism of the Feshbach projection operators is used to separate the electronic quantities needed in the first and second steps of the MQDT. We have introduced the vibrational motion within the Condon approximation. Our results lead to new unambiguous assignments of the R_B series. The vibrationally resolved cross sections, the associated branching ratios, and the background and resonant features are discussed in detail and compared with the available experimental data. There is an overall agreement between theory and experiment except for the angular distribution of photoelectrons.

I. INTRODUCTION

For forty years, the CO absorption spectrum below 20 eV has been the subject of extensive experimental work.[1–6] In this paper we shall restrict ourselves to the part of this spectral region between the CO^+ $A\,^2\Pi$ and the CO^+ $B\,^2\Sigma^+$ thresholds. In 1942, Tanaka[1] identified two Rydberg series in the 17–19.68-eV (730–630-Å) region which he called "sharp" and "diffuse" owing to their respective widths. Two new series called P_4 and P_5 have been identified by Huffmann *et al.*[3] in 1964. A reinvestigation of the spectrum led Ogawa and Ogawa[5] to classify the observed bands in four series converging to the $B\,^2\Sigma^+$ ionic state and called hereafter sharp, diffuse, III, and IV.

An atomiclike notation (e.g., $3p\sigma$, $3p\pi$, etc.) is widely used by experimentalists for the assignment of autoionizing Rydberg series. However, in molecules the potential is nonspherical and it mixes different atomic irreducible representations (IR). Therefore, the atomic IR singled out in the above notation corresponds, at best, to the atomic wave function giving the greatest contribution to the molecular channel. The other atomic IR contribute to the molecular channel to a lesser extent. To reflect this molecular situation we use the same notation as above but put the atomic IR between quotes (e.g., $3"p"\sigma$, $3"p"\pi$, etc.). If ambiguity appears concerning the ionic core to which the Rydberg state converges we add it to the above notation (for example $B3"p"\sigma$, $B3"p"\pi$, etc.).

A first assignment of these series was suggested by Lindholm[7] in 1969 (see Table I, column 2) on the basis of their quantum defects. Ogawa and Ogawa,[5] in a detailed study of the CO valence-shell absorption spectrum, observed a Q branch, in the second- and third-order spectra, for the sharp $n=3$ state: this led them to a $3"p"\pi$ assignment (Table I, column 3) in disagreement with Lindholm.[7] Fock *et al.*,[6] in their comparative study of the isoelectronic sequence BF, CO, and N_2 have reproduced Lindholm's assignments.[7]

Experimental photoionization results are also available.[8–13] Partial photoionization cross sections leading to the CO^+ $X\,^2\Sigma^+$ and $A\,^2\Pi$ states have been measured by Plummer *et al.*[10] using synchrotron radiation. Ederer *et al.*[11] have measured the asymmetry parameter for the $X\,^2\Sigma^+$ channels in the vicinity of the sharp $n=3$ resonance. Ito *et al.*[12] have measured the total photoionization spectrum and reported measurements of the A-X and B-X fluorescence cross sections. Recently, Leyh *et al.*[13] have studied the decay of these Rydberg states in the vibrational channels corresponding to the X ionic state ($v=0$–3).

A theoretical calculation of the Rydberg-state (R_B) energies has been performed by Betts and McKoy[14] using a model molecular potential calibrated to atomic data. This method did not allow them to distinguish between the different ionic cores and, moreover, the calculated quantum defects of the $3"p"\pi$ and $3"p"\sigma$ states (0.73 and 0.74) are too close to give any definite assignment. Their interpretation of the CO spectrum is summarized in Table I, column 4.

The examination of Table I leads to two conclusions.

(i) There is a disagreement between the different authors[5,6,7,14] about the $"p"\sigma$-$"p"\pi$ assignments of the sharp and diffuse series.

(ii) The interpretation of the III and IV series seems to cause fewer problems. However it is well known[15] that the assignment of the $"s"\sigma$ and $"d"\sigma$ series is not at all obvious since the quasidegenerate states $(n+1)\,s\sigma$ and $nd\sigma$ generally interact strongly.

TABLE I. Assignments of the Rydberg series converging to $CO^+ B\,^2\Sigma^+$.

	Assignments[a]				
Series	Ref. 7	Ref. 5	Ref. 14	Ref. 6	This work
Sharp	$p\sigma$	$p\pi$	$p\pi$	$p\sigma$	"p"π
Diffuse	$p\pi$	$p\sigma$	$p\sigma$	$p\pi$	"p"σ
III	$s\sigma$	$s\sigma$	$s\sigma$	$s\sigma$	"$(s-d)$"σ/"d"π
IV	$d\sigma$	$d\sigma/d\pi$	$d\pi$[b]	$d\sigma$	"$(s+d)$"σ

[a]The notation $l\lambda$ means that the l wave has the largest weight in the one-center expansion of the considered Rydberg orbital.
[b]Betts and McKoy neglect the $d\sigma$ state.

Furthermore, the detailed interpretation of the vibrational selectivity observed by Leyh *et al.*[13] needs a theoretical calculation including the vibrational motion.

To clarify this situation and to allow a detailed comparison with all the available experimental data, we performed *ab initio* calculations of the vibrationally resolved partial cross sections and of the asymmetry parameter in this region. We used a variant of the two-step multichannel quantum-defect theory (MQDT) (see Sec. II) of Giusti-Suzor and Lefebvre-Brion[16] (see also a recent review of Guisti-Suzor and Jungen[17]). The vibrational motion is introduced within the Condon approximation: this allows us to compare our results with the vibrationally resolved ones of Leyh *et al.*[13]

Up to now, no *ab initio* calculation of the electronic autoionization introducing the vibrational motion had been performed by this method. Morin *et al.*[18] have studied the vibrationally resolved O_2 photoionization spectrum restricting the number of electronic channels to two and fitting some of the electronic quantities to match the experimental spectrum. Raoult *et al.*[19] have performed a pure electronic *ab initio* study by the standard two-step MQDT on the Hopfield series in N_2.

We should also mention *ab initio* calculations of electronic autoionization by other methods especially for H_2 by Raseev[20] and for NO by Collins and Schneider.[21] The former calculation[20] uses the variational method based on the logarithmic derivative of the wave function.[22] This method is in principle applicable in the present case but at the present stage of its development it requires a calculation for each member of a Rydberg series as a discrete state. The method of Collins and Schneider[21] presently introduces only the open-channel part of the wave function; the autoionization processes are taken into account through an optical potential.

This paper is organized as follows: in Sec. II, we present a summary of the theoretical methods; Sec. III is concerned with the electronic *ab initio* calculations; in Sec. IV, we discuss these *ab initio* results as well as the MQDT differential and total cross sections; Sec. V is a conclusion.

II. REVIEW OF THE THEORETICAL APPROACH

In this section we first describe in some detail the method which we used to obtain the electronic quantities in a form suitable for the two-step MQDT. We construct, using the projection operators introduced below, a diabatic representation of the wave function. The diabatic functions are defined so as to diagonalize the nuclear kinetic energy term of the total Hamiltonian and they serve as a new basis for the representation of the MQDT wave functions. This basis-function transformation as well as the calculated electronic quantities are linked to the first step of the MQDT. The interaction between these diabatic states appears when taking into account the remaining short-range bielectronic interaction corresponding to different ionic cores and it is responsible for the electronic autoionization. The calculation of this interaction and the solution of the resulting MQDT system of equations is known as the second step MQDT. In Sec. II B the vibrational motion is taken into account within the Condon approximation (see also Morin *et al.*[18]). This vibrational motion allows us to calculate the vibrationally resolved photoionization cross section. To perform such a calculation a great number of channels must be included in the calculation owing to the heteronuclear symmetry of the molecular potential and to the different vibrational thresholds. In Sec. II C we develop a variant of the two-step MQDT which reduces the number of channels with results very close to the calculations taking into account all the channels.

The study of a photoionization spectrum of a complicated system, particularly a molecule, requires the introduction of the notion of a channel. A channel is a possible path of fragmentation of the molecule giving rise to an ion and to a continuum electron. It is labeled in part by the electronic state i and vibrational quantum number v of the ion. The label is completed by the kinetic energy $\frac{1}{2}k^2$, angular momentum l, and projection of the angular momentum onto the internuclear axis λ, of the continuum electron. We thus use the symbol $|il\lambda v\rangle$ to identify a fragmentation channel which is well characterized in the asymptotic region when the ion and the electron are well separated. The notion of channel can also be associated with the diabatic representation of the wave function and in this case is defined by $|i\beta v\rangle$ where β represents the wave functions of the excited electron which diagonalize the short-range diabatic potential. The eigenchannels corresponding to the diagonalization of the total short-range and asymptotic Hamiltonians are called $|\alpha\rangle$ and $|\rho\rangle$. Experiments can only "see" asymptotic channels $|il\lambda v\rangle$ and therefore we express the cross section in terms of these channels. The interaction takes place when all of the particles are close together. It can be expressed in a simple form in terms of the short-range eigenchannels $|i\beta v\rangle$ or $|\alpha\rangle$ and it is for this reason that the different eigenchannels are introduced. The atomiclike notation introduced in the introduction is close to the asymptotic

channel notation $|il\lambda\upsilon\rangle$. Strictly speaking this notation corresponds to the $|\alpha\rangle$ channel defined here. The $|\alpha\rangle$ channel notation will be used in this section, the atomic-like notation in the remaining sections of this paper.

A supplementary concept particular to the MQDT is the following. Short-range channels $|i\beta\upsilon\rangle$ or $|\alpha\rangle$ corresponding to the autoionizing state or to the adjacent continuum are all initially treated as open. Asymptotic channels correspond only the open channels; the effect of the closed channels is included by the MQDT elimination procedure.

A. *Ab initio* method for the calculation of the electronic quantities

In Sec. II A we ignore the vibrational motion and therefore we use channels $|il\lambda\rangle$ and $|i\beta\rangle$ or $|i\beta^{A}\rangle$ or $|i\beta(E)\rangle$ (this latter notation stresses the fact that β is defined for any positive or negative energy). The $|\alpha\rangle$ channels will consequently correspond here to the diagonalization of only the electronic part of the total Hamiltonian. However, in the rest of the paper $|\alpha\rangle$ will correspond to the diagonalization of the total Hamiltonian including vibration.

The fundamental idea underlying the methods used in the calculation of the electronic quantities of a photoionization process is the partitioning of the electronic coordinate space into two regions: the internal region (or reaction zone) usually taken as a sphere of radius r_0 centered at the center of mass of the system, and the external region. In the photoionization process described here only one electron is allowed to escape into the external region.

We partition the total Hamiltonian H into two terms, H_0 and H'. The long-range Hamiltonian H_0 of the external region contains the ionic-core Hamiltonian, the kinetic energy operator of the outer electron, and the Coulomb-interaction term between the outer electron and the ionic core. The H' Hamiltonian is a short-range interaction term which can be split into two parts, $H^{(1)}$ and $H^{(2)}$. The two steps of the MQDT correspond to successively introducing $H_0+H^{(1)}$ and then $H^{(2)}$. Both $H^{(1)}$ and $H^{(2)}$ contain part of the bielectronic repulsion term and this partition can therefore only be expressed with the help of the projection-operator formalism introduced below. The Hamiltonian $H_0+H^{(1)}$ can be viewed as an effective diabatic Hamiltonian chosen in such a way that the interaction between channels corresponding to different ionic states i is zero. $H^{(2)}$ is a short-range interacting potential between states associated with different ionic cores.

To introduce projection operators we now divide the state space corresponding to $|i\beta(E)\rangle$ into several subspaces $\mathbf{P}_i$, each corresponding to a given ionic core i. Following Feshbach[23–24] and Domcke,[25] we introduce the projection operators P_i spanning each subspace $\mathbf{P}_i$,

$$P_i=\sum_{|i\beta\rangle\in\mathbf{P}_i}\int dE\,|i\beta(E)\rangle\langle i\beta(E)|\ . \tag{1}$$

It must be mentioned that no distinction is made between the projectors associated with the bound and the continuum subspaces as in the usual Feshbach formulation.[23–24] Rather, in the usual spirit of the MQDT, the bound and continuum channels are treated on even footing. The discrete states are therefore energy normalized in the internal region. The projection operators satisfy the usual requirements

$$P_iP_{i'}=P_i\delta_{ii'} \text{ and } \sum_i P_i=1\ .$$

The partition of the Hamiltonian can now be written in the following way:

$$H=H_0+H'=H_0+H^{(1)}+H^{(2)} \tag{2a}$$

$$H^{(1)}=\sum_i P_iH'P_i,\quad \forall i \tag{2b}$$

$$H^{(2)}=\sum_i\sum_{i'(\neq i)}P_iH'P_{i'},\quad \forall i,i'\ . \tag{2c}$$

The partition of the Hamiltonian introduced above allows us to use the two-potential collision formulation of Rodberg and Thaler[26] as a framework of our model. This formulation supposes that a first potential and its corresponding wave function are known exactly. In our case this is the situation for $H_0+H^{(1)}$ and the $|i\beta\rangle$ channels. The corresponding wave equation reads

$$\begin{aligned}&(H_0+H^{(1)}-E)\,|i\beta\rangle=0\ ,\\ &|i\beta\rangle\in\mathbf{P}_i,\quad\forall i\ .\end{aligned} \tag{3}$$

For given ionic core i all of the solutions of Eq. (3) are energy degenerate. The two-potential collision formulation also supposes that the residual potential $H^{(2)}$ is weak and localized in the internal region. The Schrödinger equation corresponding to the total electronic Hamiltonian including $H^{(2)}$ is not known exactly. We can write it formally in terms of $|\alpha\rangle$ channels

$$(H_0+H'-E)\,|\psi_{\alpha E}\rangle=0\ . \tag{4}$$

What we want now is to obtain an expression of $\psi_{\alpha E}$ in terms of known $|i\beta\rangle$ channels. Following Rodberg and Thaler[26] we multiply (3) by $\psi_{\alpha E}$, (4) by $|i\beta\rangle$, integrate, and perform a few standard algebraic manipulations to obtain an integral form of the wave function,

$$\begin{aligned}\psi_{\alpha E}(r)=&\sum_{|i\beta\rangle\in\mathbf{P}_i}|i\beta\rangle\langle i\beta|\alpha\rangle\cos(\pi\mu_\alpha)\\ &-W^{-1}\Big[\,|\overline{i\beta}\rangle\int_0^r\langle i\beta|H^{(2)}\psi_{\alpha E}(r')dr'\\ &-|i\beta\rangle\int_r^\infty\langle\overline{i\beta}|H^{(2)}\psi_{\alpha E}(r')dr'\Big]\ .\end{aligned} \tag{5}$$

In (5) $|\overline{i\beta}\rangle$ are the irregular functions associated with the regular $|i\beta\rangle$ functions and W is the Wronskian of these functions. The factors $\langle i\beta|\alpha\rangle$ and $\cos(\pi\mu_\alpha)$ are obtained from the diagonalization of the $K^{(2)}$ matrix introduced below [Eq. (6)]. In (5) we have made no approximations. In particular $\psi_{\alpha E}(r)$ is valid for any value of r and at an

energy E there are as many $\psi_{\alpha E}$ wave functions as the dimension of the total space.

To obtain a tractable approximate wave function in the external region we remember the characteristics of the $H^{(2)}$ potential, namely, its weakness and its localization in the internal region. Therefore, for r not too small, we can neglect the second integral in (5) (strictly speaking this is true for $r > r_0$). We then introduce expression (1) for the projection operators into the expression (2c) for $H^{(2)}$ and the resulting expression of $H^{(2)}$ in the remaining integral in Eq. (5). Finally, Eq. (5) for $\psi_{\alpha E}$ is iteratively inserted into the integral on the right-hand side of this equation, giving rise to an infinite perturbation expansion. We condense this expansion in the $\bar{K}^{(2)}$ operator. The wave function $\psi_{\alpha E}(r)$ valid exactly in the external region now reads

$$\psi^{\Lambda}_{\alpha E} \underset{r>r_0}{\rightarrow} \sum_{|i\beta\rangle \in \mathbb{P}_i} \sum_{\substack{|i'\beta'\rangle \in \mathbb{P}_{i'} \\ (i' \neq i)}} (|i\beta\rangle \delta_{i\beta,i'\beta'} - W^{-1}|\bar{i}\bar{\beta}\rangle\langle i\beta|\bar{K}^{(2)}|i'\beta'\rangle)\langle i'\beta'|\alpha\rangle \cos(\pi\mu_\alpha) . \tag{6}$$

We define the $K^{(2)}$ matrix by the expression

$$K^{(2)}_{i\beta,i'\beta'} = \langle i\beta|\bar{K}^{(2)}|i'\beta'\rangle \sim \langle i\beta|H'|i'\beta'\rangle . \tag{7}$$

The integral over r in Eq. (7) is restricted to the internal region $r < r_0$. The last equality is the first-order approximation to the $K^{(2)}$ matrix which will be used in this paper. The $K^{(2)}$ matrix has a particular structure, in that its diagonal submatrices, each of the same dimension as the corresponding subspace $\mathbb{P}_i$, are zero. This is due to the particular form of the $H^{(2)}$ operator and Eq. (3) which together eliminate the interaction in a particular P_i subspace.

Equation (3) corresponds to the first step of the MQDT whereas the second term in (6) or the matrix $K^{(2)}$ corresponds to the second step of the MQDT.

We briefly describe now the method we used to obtain the above-mentioned $|i\beta\rangle$ states. Each state is represented by a one-configuration wave function which is an eigenfunction of given spin and symmetry and which is called a configuration state function (CSF),

$$|i\beta^{\Lambda}\rangle = \mathscr{A}[\Phi_i^{\Lambda^+}(\rho) f^{\lambda}_{\beta}(\nu_i, r)] . \tag{8}$$

In (8), $\mathscr{A}$ is the antisymmetrization operator, $\Phi_i^{\Lambda^+}(\rho)$ is the wave function of the ionic core i, and ρ are the coordinate of the $N-1$ electrons. The function $f^{\lambda}_{\beta}(\nu_j, r)$ is the wave function of the excited or continuum electron. In (8), $|i\beta^{\Lambda}\rangle$ is represented for simplicity as a single Slater determinant. In fact $|i\beta^{\Lambda}\rangle$ can also, in some cases, take the form of a sum of Slater determinants. For a diatomic molecule we have $\Lambda = \Lambda^+ + \lambda$ where Λ^+, λ, and Λ represent, respectively, the projection on the internuclear axis of the electronic angular momentum of the ion, of the continuum electron, and of the total N-particle system. ν_i is the effective principal quantum number related to the photoelectron energy by the relation $\epsilon_i = -1/2\nu_i^2$.

Before solving (3) let us rewrite it in a modified form. Using the orthogonality properties of the projection operators, we obtain

$$\langle i\beta'|H - E|i\beta\rangle = 0 . \tag{3'}$$

We now solve (3') with the use of (8) which corresponds to the calculation of the first-step MQDT electronic quantities. We calculate f^{λ}_{β} in the frozen-core static-exchange (FCSE) approximation. This allows us to determine f^{λ}_{β} when the ion state wave function is known and assumed unchanged by the interaction with f^{λ}_{β}. The function f^{λ}_{β} can correspond to either a continuum state (open channel) or to a discrete state (closed channel).

If $|i\beta\rangle$ is an open channel, we expand the eigenchannel form f^{λ}_{β} of the continuum electron wave function in spherical harmonics[29,30]

$$f^{\lambda}_{\beta}(\nu_i, r) = \sum_{l'=|\lambda|}^{\infty} \sum_{l=|\lambda|}^{\infty} Y_{l\lambda}(\hat{r}) f^{\lambda}_{l'}(\nu_i, r) \times \langle l'\lambda|\beta\rangle \cos(\pi\mu_\beta) . \tag{9}$$

In (9), the radial wave functions $f^{\lambda}_{l'}$ are solutions of a close-coupling system of equations and $\langle l\lambda|\beta\rangle$ and μ_β are the mixing coefficients and the eigenphases resulting from the diagonalization of the $K^{(1)}$ matrix corresponding to the Hamiltonian $H_0 + H^{(1)}$. The close-coupling system is obtained by expanding, in Eq. (5), the Hamiltonian $H_0 + H^{(1)}$ in spherical harmonic together with the bound orbitals η_l of the $\phi_i^{\Lambda^+}(\rho)$ ion wave function (8) and the continuum functions (9).[29-30] The main problem in this approach is related to the cutoff of the different multipolar expansions: of the continuum wave function f^{λ}_{β} (the maximum value is $l^c_{\max}$), of the bound orbitals η_j ($l^b_{\max}$), and of the potential corresponding to Hamiltonian $H_0 + H^{(1)}$, especially of the inverse of the interelectronic distance appearing in the static ($\gamma^{st}_{\max}$) and the exchange ($\gamma^{ex}_{\max}$) interactions. These cutoffs are essential to keep the close-coupling system of equations tractable. They are particular to each example treated and the one retained in the CO case are discussed in Sec. III.

In the case when the channel $|i\beta\rangle$ is closed it is associated with a Rydberg series converging to a given ionic state i. The corresponding molecular wave function f^{λ}_{β} of the excited electron is expanded in terms of a set of known bound atomic orbitals $\chi_p(r)$ (Ref. 31) and $C_{p\beta}$ expansion coefficients

$$f^{\lambda}_{\beta}(\nu_i, r) = N_{E_i} \sum_p \chi_p(r) C_{p\beta} . \tag{10}$$

The normalization constant N_{E_i} is obtained as follows. The energy of a Rydberg state can be fitted to the Rydberg formula $E_i = -1/2\nu_i^2$. The effective quantum number ν_i is given by $\nu_i = n - \mu_\beta$ where n is the principal

quantum number and μ_B the quantum defect associated with $f^{\lambda}_{\beta}(\nu_l,r)$. The normalization constant N_E is equal to the inverse of $(dE/d\nu_i)^{1/2}$, i.e., to $\nu_i^{3/2}$.

We now specify the form of $K^{(2)}$ in the present framework. The first-order approximation used in (7) is valid in the case of weak electrostatic interactions (e.g., for the autoionization of Rydberg states as in our case). In the one-configuration approximation (8), the $K_{i\beta,i'\beta'}$ matrix element reduces to a sum of two two-electron integrals.

The transition dipole amplitude for a transition from an initial state having the one-configuration wave function $\psi^{\Lambda''}$ to a final state $|i\beta\rangle$ has the following form:

$$D^{\Lambda'\leftarrow\Lambda''}_{i\beta}=\langle i\beta^{\Lambda'}|\mu|\psi^{\Lambda''}\rangle . \tag{11}$$

Note that in Eq. (11) the angular momentum Λ of the final state has been changed to Λ' to be consistent with the spectroscopic notation. The transition amplitude (11) is calculated exactly in the framework of one-configuration representation, ignores autoionization, and corresponds to the first step of the MQDT. The transition amplitude from the initial state $\psi^{\Lambda''}$ to the final state $|\alpha\rangle$ written in the form of Eq. (6) will include autoionization. Presently, however, we are unable to perform the integral corresponding to the second term of (6). Therefore we neglect it and, to preserve normalization, we also take $\cos(\pi\mu_\alpha)=1$. These approximations are justified in the case of weak $H^{(2)}$ interaction. The resulting expression below will still introduce autoionization through the coefficients $\langle i\beta|\alpha\rangle$ which mixes resonant and continuum channels. The transition amplitude to a final channel $|\alpha\rangle$ then reads

$$D^{\Lambda'\leftarrow\Lambda''}_{\alpha}=\langle\psi^{\Lambda'}_{E}|\mu|\psi^{\Lambda''}\rangle=\sum_{|i\beta\rangle}\langle i\beta|\alpha\rangle D^{\Lambda'\leftarrow\Lambda''}_{i\beta} . \tag{11'}$$

Finally, an approximation is also used in the calculation of $D^{\Lambda'\leftarrow\Lambda''}_{i\beta}$, namely, the same molecular orbitals are used for the ionic core $\phi_i^{\Lambda^+}$ and the initial state $\psi^{\Lambda''}$ wave functions, thus allowing us to write the transition moment as

$$D^{\Lambda'\leftarrow\Lambda''}_{i\beta}=\langle f^{\lambda}_{i\beta}|\mu|\phi^{\rm in}\rangle ,$$

where $\phi^{\rm in}$ is the initial orbital from which the electron is ejected. Note the we have added to f^{λ}_{β} an index i to specify to which ionic core it corresponds.

B. Inclusion of the vibrational motion within the Condon approximation

In Sec. II B, we introduce the vibrational motion within the Condon approximation, i.e., we assume that the electronic quantities vary slowly with the internuclear distance. As stated in the beginning of Sec. II, we use in the following $|il\lambda v\rangle$, $|i\beta v\rangle$, and $|\alpha\rangle$ channels. Particularly the $|\alpha\rangle$ channels, will now include a vibrational function corresponding to a linear combination of pure vibrational wave functions $|iv\rangle$.

We can construct the analog of the $K^{(2)}$ electronic matrix [Eqs. (7)] as follows:

$$\begin{aligned}K^{(2)}_{i\beta v,i'\beta'v'}&=\langle i\beta v|K^{(2)}|i'\beta'v'\rangle\\&=\langle iv|i'v'\rangle\langle i\beta|K^{(2)}|i'\beta'\rangle\\&=\langle iv|i'v'\rangle\langle i\beta|H'|i'\beta'\rangle .\end{aligned} \tag{12}$$

Note that, for a given ionic core, $\langle i\beta|H^{(2)}|i\beta'\rangle=0$ and that the associated vibrational overlaps are $\langle iv|iv'\rangle=\delta_{vv'}$. Therefore the $K^{(2)}$ matrix of Eq. (12) has the same block-diagonal structure as the electronic $K^{(2)}$ matrix of Sec. II A.

The electronic-transition amplitude [Eq. (11)] must also be multiplied by the overlaps between the initial $|i_0v_0\rangle$ and the final $|iv\rangle$ state vibrational functions

$$D^{v_0}_{\alpha}=\sum_{i,\beta,v}\langle i\beta v|\alpha\rangle D^{\Lambda'\leftarrow\Lambda''}_{i\beta}\langle iv|i_0v_0\rangle . \tag{13}$$

A consequence of introducing the vibrational motion is the increase of the number of asymptotic channels. Namely, each electronic channel is replaced by n_v vibronic channels, n_v being the number of vibrational levels which have been considered for this electronic ionic state. The electronic thresholds are shifted by the vibrational energies of the different vibrational levels.

It is worthwhile to note that in the Condon approximation we cannot take into account the vibrational autoionization, i.e., the direct interaction between different vibrational channels corresponding to the same ionic core. However, these channels interact indirectly through their respective coupling with the channels associated with a different ionic core.

C. Summary of the two-step MQDT

As stated in the Introduction, the two-step MQDT has been exclusively discussed in recent papers (see Raoult *et al.*,[19] Giusti-Suzor and Jungen,[17] Giusti-Suzor and Fano,[27] and Greene and Jungen[32]). It is an external-region theory which takes advantage of internal-region calculations. In the following we give a variant of the two-step MQDT which is more efficient in the case of many electronic and vibrational channels.

The connection between the present section and the preceding ones is made through the asymptotic forms of the wave functions. Namely, we start from Eq. (6) and replace $|i\beta^{\Lambda}\rangle$ by a product (antisymmetry is not needed asymptotically) of ionic core and excited electron wave functions [see Eq. (8)]. We then include vibrational motion and also replace each wave function by its asymptotic form to obtain

$$\psi^{\Lambda}_{\alpha E}=\sum_{l}\sum_{|i\beta v\rangle\in P_l}\Phi_i^{\Lambda^+}(\rho)\chi_{iv}(R)[f^{\lambda}_{\beta}(\nu_{iv},r)\langle i\beta v|\alpha\rangle\cos(\pi\mu_\alpha)-g^{\lambda}_{\beta}(\nu_{iv},r)\langle i\beta v|\alpha\rangle\sin(\pi\mu_\alpha)] \quad \text{for } r>r_0 \tag{14}$$

where

$$f_\beta^\lambda(\nu_{i\upsilon},r)=\sum_l Y_{l\lambda}(\hat{r})[f_{l\lambda}(\nu_{i\upsilon},r)\langle l\lambda\,|\,\beta\rangle\cos(\pi\mu_\beta)-g_{l\lambda}(\nu_{i\upsilon},r)\langle l\lambda\,|\,\beta\rangle\sin(\pi\mu_\beta)]\ ,$$

$$g_\beta^\lambda(\nu_{i\upsilon},r)=\sum_l Y_{l\lambda}(\hat{r})[f_{l\lambda}(\nu_{i\upsilon},r)\langle l\lambda\,|\,\beta\rangle\sin(\pi\mu_\beta)+g_{l\lambda}(\nu_{i\upsilon},r)\langle l\lambda\,|\,\beta\rangle\cos(\pi\mu_\beta)]\ . \tag{15}$$

Note that f_β^λ and g_β^λ are regular and irregular wave functions of the excited electron. The other quantities appearing in Eq. (15) have previously been defined. In Eq. (14) the first-step interaction corresponding to μ_β is hidden. Giusti-Suzor and Lefebvre-Brion[16] introduce (15) into (14) and write the resulting equations in terms of $|\,il\lambda\upsilon\rangle$ channels. We also introduce (15) into (14) but instead write the resulting equations in terms of $|\,i\beta\upsilon\rangle$ channels,

$$\psi_{\alpha E}^\Lambda=\sum_{i,\beta,\nu}\phi_i^{\Lambda^+}(\rho)\chi_{i\upsilon}(R)[f_\beta^{\lambda(0)}(\nu_{i\upsilon},r)\mathscr{C}_{i\beta\upsilon,\alpha}^\Lambda - g_\beta^{\lambda(0)}(\nu_{i\upsilon},r)\mathscr{S}_{i\beta\upsilon,\alpha}^\Lambda]\ , \tag{16}$$

where

$$f_\beta^{\lambda(0)}(\nu_{i\upsilon},r)=\sum_l Y_{l\lambda}(\hat{r})f_{l\lambda}(\nu_{i\upsilon},r)\langle l\lambda\,|\,\beta\rangle\ ,$$

$$g_\beta^{\lambda(0)}(\nu_{i\upsilon},r)=\sum_l Y_{l\lambda}(\hat{r})g_{l\lambda}(\nu_{i\upsilon},r)\langle l\lambda\,|\,\beta\rangle\ ,$$

and

$$\mathscr{C}_{i\beta\upsilon,\alpha}^\Lambda=\langle i\beta\upsilon\,|\,\alpha\rangle\cos[\pi(\mu_\beta+\mu_\alpha)]\ ,$$

$$\mathscr{S}_{i\beta\upsilon,\alpha}^\Lambda=\langle i\beta\upsilon\,|\,\alpha\rangle\sin[\pi(\mu_\beta+\mu_\alpha)]\ .$$

In Eq. (16), the angular term corresponding to the r vector usually included in $\phi_i^{\Lambda^+}$, is now included in $f_\beta^{\lambda(0)}$ and $g_\beta^{\lambda(0)}$. We can write the asymptotic forms of the wave function in terms of the $|\,i\beta\upsilon\rangle$ open and closed channels; these forms are similar to the corresponding expressions in terms of the $|\,il\lambda\upsilon\rangle$ channels (see, e.g., Fano[33] and Jungen and Dill[34]).

The MQDT performs linear combinations of these internal region solutions $\psi_{\alpha E}^\Lambda$ of the Schrödinger equation which take into account the asymptotic convergence condition for the closed channels and the incoming wave normalization for the open channels. We then obtain the MQDT system of equations[33,35] by identifying these linear combinations of the $\psi_{\alpha E}^\Lambda$ solutions [Eq. (16)] and the asymptotic expressions. This system is written in a slightly different form from that of Greene and Jungen:[32] the eigenvalues are expressed as $\cot(\pi\tau_\rho)$ instead of $\tan(\pi\tau_\rho)$,

$$\sum_{\alpha\in P\otimes Q}[\mathscr{C}_{i\beta\upsilon,\alpha}^\Lambda - \cot(\pi\tau_\rho)\mathscr{S}_{i\beta\upsilon,\alpha}^\Lambda]A_{\alpha\rho}=0,\quad i\beta\upsilon\in P \tag{17a}$$

$$\sum_{\alpha\in P\otimes Q}[\sin(\pi\nu_{i\upsilon})\mathscr{C}_{i\beta\upsilon,\alpha}^\Lambda + \cos(\pi\nu_{i\upsilon})\mathscr{S}_{i\beta\upsilon,\alpha}^\Lambda]A_{\alpha\rho}=0,\quad i\beta\upsilon\in Q \tag{17b}$$

where τ_ρ are the eigenphases of the effective open-channel matrices K or S and $A_{\alpha\rho}$ are the projections of the $|\,\rho\rangle$ asymptotic channels into the α internal-region eigenchannels. P contains all the open vibronic channels. Q represents the subspace of the closed channels. Following Greene and Jungen,[32] we write (17) as a generalized eigenvalue equation,

$$\underline{\Delta}\,\underline{A}=\underline{\theta}\,\underline{A}\,\underline{b}\ , \tag{18}$$

where $\Delta_{i\beta\upsilon,\alpha}=\mathscr{C}_{i\beta\upsilon,\alpha}^\Lambda$ and $\theta_{i\beta\upsilon,\alpha}=\mathscr{S}_{i\beta\upsilon,\alpha}^\Lambda$ when $i\beta\upsilon\in P$ and $\Delta_{i\beta\upsilon,\alpha}=\sin(\pi\nu_{i\upsilon})\mathscr{C}_{i\beta\upsilon,\alpha}^\Lambda+\cos(\pi\nu_{i\upsilon})\mathscr{S}_{i\beta\upsilon,\alpha}^\Lambda$ and $\theta_{i\beta\upsilon,\alpha}=0$ when $i\beta\upsilon\in Q$. Note that $b_{\rho\rho'}=\delta_{\rho\rho'}\cot(\pi\tau_\rho)$.

In Eq. (18) we simultaneously obtain all of the eigenvalues b_ρ and eigenvectors A_ρ. This was not the case with the previous algorithms which obtained each eigenvalue separately. The new procedure is particularly useful in the case of degenerate or nearly degenerate eigenvalues. In Eq. (18) the eigenvectors A do not correspond to the eigenvectors of the effective K or S matrix. The orthogonal eigenvectors $\langle i\lambda\upsilon\,|\,\rho\rangle$ of the effective S matrix are obtained from the following equation [similar to Eq. (15b) of Jungen and Dill[33]]:

$$\langle il\lambda\upsilon\,|\,\rho\rangle=\sum_{i\beta)\in P}\langle il\lambda\,|\,i\beta\rangle \times\sum_{\alpha\in P\otimes Q}[\mathscr{C}_{i\beta\upsilon,\alpha}^\Lambda A_{\alpha\rho}\sin(\pi\tau_\rho) + \mathscr{S}_{i\beta\upsilon,\alpha}^\Lambda A_{\alpha\rho}\cos(\pi\tau_\rho)]\ . \tag{19}$$

It can be demonstrated (see Greene and Jungen[32]) that the $\langle il\lambda\upsilon\,|\,\rho\rangle$ eigenvectors obtained from Eq. (19) are orthogonal, leading to symmetric K and S matrices. If some eigenvalues of (18) are strictly degenerate, the corresponding eigenvectors obtained from (19) are not necessarily orthogonal. In this case, we have the freedom to orthogonalize them.

Finally, the complex transition moment which is used in the calculation of the cross sections and angular distributions (see, e.g., Starace,[28] Fano and Dill,[36] Dill and Dehmer,[37] Raoult *et al.*[19]) is

$$D_{il\lambda\upsilon}^{(-)}=\sum_{\rho\in P}\langle il\lambda\upsilon\,|\,\rho\rangle e^{i\pi\tau_\rho} \times\sum_{\alpha\in P\otimes Q}A_{\alpha\rho}D_\alpha^{\upsilon_0}\ . \tag{20}$$

Let us now comment on our variant of the two-step MQDT. In (14) the first-step interaction corresponding to μ_β is hidden and therefore we can not use this formulation directly. On the contrary, in Eq. (16) the quantum defects μ_β and μ_α are explicitly present in the $\mathscr{C}_{i\beta\upsilon}^\Lambda$ and $\mathscr{S}_{i\beta\upsilon}^\Lambda$ coefficients which are used in (18) to obtain the asymptotic quantum defects τ_ρ corresponding to the effective S matrix. The eigenchannels τ_ρ then condense asymptotically the entire electronic interaction corresponding to $H_0+H^{(1)}$ and to $H^{(2)}$. It follows, therefore, that the present formulation gives the same results as the standard

two-step MQDT formulation.

So far we have shown that the two formulations are identical. The advantage of the present variant is that we can work with a number of $|i\beta v\rangle$ channels which is smaller than the number of $|il\lambda v\rangle$ channels. This is possible if some of the quantum defects μ_β and transition moments $D_{i\beta}^{\Lambda'\leftarrow\Lambda''}$ are very small. Then reducing the $|i\beta v\rangle$ space corresponds to setting these quantum defects and transition moments equal to zero. Solving (18) in the reduced space is more efficient than solving the standard MQDT system in terms of the complete $|il\lambda v\rangle$ space. The effect of this reduction on the cross sections and angular distributions of the photoelectrons will be negligible.

III. FRAMEWORK OF THE *ab initio* CALCULATIONS

In this section we show how we calculated the *ab initio* quantities used in the two-step MQDT. This is performed following the general discussion of Sec. II. We distinguish two steps. The first step is the calculation involving each subspace $\mathbb{P}_i$ individually, the second step is the calculation of the interactions between these subspaces, giving rise to the electronic autoionization.

A. Calculations for individual $\mathbf{P}_i$ subspaces

The present calculations are performed in the framework of the one configuration FCSE approximation. As mentioned in Sec. II, the calculation uses different methods depending on whether the energy of the excited electron is positive (continuum case [Eq. (9)]) or negative (bound case [Eq. (10)]).

In the case of a continuum electron, we have used the one-center method developed by Raşeev *et al.*[29,30] The static potentials of the outer electron in the field of each ionic core have been built on the CO $X\,^1\Sigma^+$ ground-state orbitals (at the equilibrium internuclear distance, $R=2.132$ a.u.). Two different basis sets have been used. The first one[38] consists of eight σ and four π Slater orbitals, including $3d\sigma$ and $3d\pi$, on each nucleus. The second one is the basis set optimized by McLean and Yoshimine[39] which provides near-Hartree-Fock results. Electronic quantities obtained with these two basis sets are compared in Table II.

The main problem arising in the computation of the continuum wave functions is the cutoff of the different one-center expansions appearing in the coupled differential equations derived from the Schrödinger equation.[29,30] For the convergence of the static potential a previous study[40] on the e^--N_2 collision suggested that a good compromise between accuracy and reasonable computer costs could be obtained with the following parameters: 20 terms in the expansion of the bound orbitals, 14 terms for the electron-electron potential, and 26 terms for the electron-nuclei potentials. The estimated accuracy is of about 2%.[40]

We have studied the convergence of the multipolar expansion of the continuum orbital [see Eq. (9) and the discussion following it in Sec. II] when we only take into account the static potential. A previous work[29] on the N_2 photoionization showed that at least ten terms are necessary to obtain accurate results. Calculations were performed with $l^c_{\max}=10$ and 12 (see Table III). The discrepancies between the two types of calculations is at most 0.01 for the quantum defects and we have consequently performed all our calculations with $l^c_{\max}=10$.

For the exchange interaction only we have further reduced the number of terms in the continuum and bound orbital expansions. The cutoff of these expansions together with the cutoff $\gamma^{\rm ex}_{\max}$ of the exchange interactions, (see Sec. II) has been studied carefully at the following kinetic energies:

$X\,^2\Sigma^+\varepsilon\sigma$: $\varepsilon_k=0.005$, 0.40, and 0.51 a.u. ,

$B\,^2\Sigma^+\varepsilon\sigma$: $\varepsilon_k=0.005$ a.u. ,

$B\,^2\Sigma^+\varepsilon\pi$: $\varepsilon_k=0.005$ a.u. ,

leading to the results summarized in Table IV. Reasonable results can be obtained with $\gamma^{\rm ex}_{\max}=4$, $l^{b,{\rm ex}}_{\max}=l^{c,{\rm ex}}_{\max}=6$. Calculations including the exchange potential have also been performed with $l^c_{\max}=12$ without modifying the previous conclusions.

The results obtained with the two different basis sets do not show any significant discrepancy. In the following, we shall only refer to results obtained with the McLean-Yoshimine[39] basis set.

It is well known that strong oscillator strengths associated with the transitions to the antibonding π^* orbital (particularly the $\pi\rightarrow\pi^*$ transition) perturb the cross sections corresponding to the $\epsilon\pi$ channels.[41] Different methods to overcome these spurious effects have been reported.[41] It seemed to us that the most convenient method in the one-configuration approximation is to orthogonalize all of the $\epsilon\pi$ orbitals with respect to the π^* orbital (which is obtained as an eigenfunction of the singlet neutral Hartree-Fock potential). The influence of this

TABLE II. Energies, dipole moments, and quadrupole moments of CO and CO^+ at $R_{CO}=2.132$ a.u. All dipole and quadrupole moments are given in atomic units (a.u.), at the center of mass of the nuclei. The positive axis is $C\rightarrow O$.

	$8\sigma/4\pi$ basis set (Ref. 38)	McLean-Yoshimine basis set (Ref. 39)
Energy (a.u.) of CO $X\,^1\Sigma^+$	−112.7793450	−112.7891398
Dipole moment of CO $X\,^1\Sigma^+$	−0.1665	−0.1123
Quadrupole moment of CO $X\,^1\Sigma^+$	−1.3854	−1.6377
Dipole moment of CO^+ $X\,^2\Sigma^+$	−1.8830	−1.8061
Quadrupole moment of CO^+ $X\,^2\Sigma^+$	2.2933	2.1490

TABLE III. Convergence of the one-center expansions without taking into account the exchange potentials.

l^c_{max}	Quantum defects "s"	"p"	"d"	"f"	Electronic cross section (Mb)
(a) $X\,^2\Sigma^+$ $\epsilon\sigma$; $\varepsilon_k=0.005$ a.u.					
10	−0.1355	0.1900	−0.1770	0.0066	0.7058
12	−0.1291	0.1911	−0.1764	0.0179	0.7195
(b) $B\,^2\Sigma^+$ $\epsilon\sigma$; $\varepsilon_k=0.005$ a.u.					
10	−0.3835	0.4210	−0.1503	0.0205	1.1915
12	−0.3821	0.4261	−0.1479	0.0205	1.2163

orthogonalization is dramatic for the $A\,^2\Pi$ $\epsilon\pi$ channel as already reported by Lucchese *et al.*[41] for the isoelectronic N_2 case. There the corresponding cross section is reduced by a factor of 10. Our results show that the cross sections of $X\,^2\Sigma^+$ $\epsilon\pi$ and $B\,^2\Sigma^+$ $\epsilon\pi$ are also modified but in a less dramatic manner: at the threshold, the ratio of the partial cross sections, calculated with and without orthogonalization to π^*, are 0.4 and 1.4, respectively. The consequences for the asymmetry parameter are discussed in Sec. IV.

In the case of a Rydberg electron we have used a method developed by Lefebvre-Brion[31] which consists of a bound-type calculation followed by an energy normalization [see Eq. (10)]. The Rydberg orbital is the nth natural orbital arising from a configuration-interaction (CI) calculation including all of the monoexcited configurations which leave the ionic core frozen. By this method, the Rydberg orbital is calculated at the same level of approximation (FSCE) as the continuum one.

To represent the Rydberg states, 18 atomic diffuse Slater orbitals centered on the center of mass have been introduced in the valence basis set of McLean and Yoshimine.[39] The exponents of these orbitals are calculated using the formula

$$\zeta=\frac{1}{n-\mu}\ ,$$

where μ is one of the quantum defects given in Table V. These quantum defects are obtained either by extrapolation from the continuum or from Rydberg formula with the energy taken from the experimental spectrum. The actual quantum defect will be a modified one obtained by the calculation.

B. Interactions between different $\mathbb{P}_i$ subspaces

The $\mathbb{P}_i$-$\mathbb{P}_j$ interactions providing the second step $K^{(2)}_{i\beta,i'\beta'}$ matrix of Eq. (7) are first calculated as bound-continuum interactions[42] and then energy renormalized using the N_{E_i} coefficient of Eq. (10). The bound states we

TABLE IV. Convergence of the multipolar expansions of the exchange potential.

γ^{ex}_{max}	$l^{b,ex}_{max}$	$l^{c,ex}_{max}$	Quantum defects "s"	"p"	"d"	"f"
(a) $X\,^2\Sigma^+ + \epsilon\sigma$; $\varepsilon_k=0.005$ a.u., $l^c_{max}=10$						
2	4	4	−0.1718	−0.4427	−0.0302	0.0452
2	6	6	−0.1745	−0.4438	−0.0315	0.0086
4	6	6	−0.1717	−0.4409	−0.0322	0.0075
(b) $X\,^2\Sigma^+ + \epsilon\sigma$; $\varepsilon_k=0.40$ a.u., $l^c_{max}=10$						
4	6	6	−0.3869	0.2968	−0.0124	0.2048
6	6	6	−0.3855	0.2973	−0.0121	0.2006
(c) $X\,^2\Sigma^+ + \epsilon\sigma$; $\varepsilon_k=0.51$ a.u., $l^c_{max}=10$						
4	6	6	−0.4194	0.2414	0.0104	0.3001
6	6	6	−0.4179	0.2407	0.0107	0.2972
(d) $B\,^2\Sigma^+ + \epsilon\sigma$; $\varepsilon_k=0.005$ a.u., $l^c_{max}=10$						
2	6	6	0.1184	0.4452	−0.1456	0.0204
4	6	6	0.1262	0.4509	−0.1420	0.0207
6	6	6	0.1270	0.4515	−0.1411	0.0208
(e) $B\,^2\Sigma^+ + \epsilon\pi$; $\varepsilon_k=0.005$ a.u., $l^c_{max}=10$						
2	6	6	−0.3838	−0.1496	0.0197	
4	6	6	−0.3613	−0.1304	0.0199	
6	6	6	−0.3566	−0.1256	0.0199	

TABLE V. Quantum defects used in the calculation of the Rydberg orbitals.

Orbital	$s\sigma$	$p\sigma$	$d\sigma$	$p\pi$	$d\pi$	$d\delta$
μ	0.940	0.580	0.200	0.680	0.130	0.040

have considered are the first member of each Rydberg series except for the "s" series where 3"s"σ has not been considered. All of the interactions are calculated at the energy of the corresponding Rydberg state; we have neglected the energy dependence of these quantities as the spectral region studied is small.

C. Vibrational motion

Within the Condon approximation, the electronic quantities discussed above are assumed to be independent of the internuclear distance R. All of the R dependence is then contained in the $\langle iv \mid i'v' \rangle$ overlap integrals. The nuclear potentials have been approximated by Morse potentials with the values of $\omega_e, \omega_e x_e$, and R_e taken from Huber and Herzberg.[43] The overlap integrals are calculated with a program written by Felenbok.[44]

IV. RESULTS

The present section is divided into Secs. IV A–IV D. In the first of these we discuss our assignments of the Rydberg series converging to CO^+ $B\,^2\Sigma^+$. These assignments are compared with the previous ones.[5–7,14] Sec. IV B is concerned with the MQDT partial photoionization cross sections, i.e., cross sections which are not vibrationally resolved. The vibrationally resolved cross sections for the $X\,^2\Sigma^+$ state are presented in Sec. IV C. These cross sections were calculated neglecting the vibrational structure at the $A\,^2\Pi$ ionic state. Section IV D deals with the angular-distribution results.

The quantum defects, transition moments, and mixing coefficients corresponding to the 31 electronic eigenchannels retained in the calculations were obtained at an energy of 17.3 eV for the Σ channels and 17.1 eV for the Π channels. These calculations were done using the method described in Sec. II following the procedures presented in Sec. III. The quantum defects and the transition moments corresponding to the $B\,^2\Sigma^+$ $\epsilon\sigma$ and $\epsilon\pi$ channels were derived from the Rydberg-state calculations whereas the corresponding mixing coefficients were calculated at a slightly positive electron energy (0.1 eV).

A. Assignments of the Rydberg series converging to CO^+ $B\,^2\Sigma^+$

In Table VI, we display the energy positions and quantum defects of the Rydberg series converging to the $B\,^2\Sigma^+$ ionic state (R_B series). The quantum defects are either obtained from the discrete-state calculations (Rydberg formula) or by linear extrapolation of the continuum phase shifts into the discrete energy range. These quantum defects and transition moments agree within a precision of about 10% with those linearly extrapolated from the corresponding continuum quantities. These results are compared with the experimental ones of Ogawa and Ogawa.[5] The decay widths, calculated in the framework of the Fermi golden rule are given in Table VI for some of these Rydberg states.

The good agreement between our results and the experi-

TABLE VI. Energies and widths of the Rydberg states converging to CO^+ $B\,^2\Sigma^+$.

Series	Assignments[a]	Energies (eV) Theor.[b]	Energies (eV) Expt.[c]	Quantum defects Theoretical Direct[e] Calc.	Quantum defects Theoretical Linear[f] extrapolation	Quantum defects Expt.[c]	Theor. widths (eV)
	$3s\sigma$	16.198	16.30[d]	1.021	1.094		0.0682
Sharp	$3p\pi$	17.150	17.089	0.677	0.739	0.705	0.0409
Diffuse	$3p\sigma$	17.384	17.302	0.561	0.521	0.604	0.0492
IV	$(4s+3d)\sigma$	18.036	17.943	1.116	1.113	1.195	0.0125
	$3d\pi$	18.268		−0.113	−0.116		0.0155
III			18.202			−0.042	
	$(4s\text{-}3d)\sigma$	18.268		−0.113	−0.095		0.0262
Sharp	$4p\pi$	18.463	18.438	0.645	0.697	0.679	0.0171
Diffuse	$4p\sigma$	18.561	18.482	0.500	0.487	0.619	0.0313
IV	$(5s+4d)\sigma$	18.749	18.729	1.161	1.120	1.202	
	$4d\pi$	18.853		−0.076	−0.119		
III			18.844			−0.054	
	$(5s\text{-}4d)\sigma$	18.854		−0.078	−0.113		

[a]Only the major components of the linear combination of atomic orbitals expansions are given. The quote notation is not used.
[b]Calculated by the method of Lefebvre-Brion (Ref. 31).
[c]From Ogawa and Ogawa (Ref. 5) ($v=0$ states).
[d]From Fock *et al.* (Ref. 6).
[e]Derived from the theoretical energies using the Rydberg formula.
[f]Extrapolation of the continuum phase shifts (divided by π).

mental data—the energies differ by at most 0.09 eV—led us to suggest the assignments which were given in the last column of Table I. The calculated widths of the "p"π states are smaller than those of the "p"σ states in agreement with the historical assignments of these two series. However, the absolute values of these widths are twice as large as the experimental[3] ones.

The series III and IV has strong s-d mixing which varies very slowly with energy. We have therefore labeled them "$[(n+1)s \pm nd]$"σ. This mixing, which is quite common in molecules such as NO and N_2, was discussed for the first time by Jungen.[15] In our case the s-d mixing for the "$s+d$" states is 62% (s), 31% (d), and 9% (p). This p character results from the heteronuclear component of the molecular field. In the "s-d" states, the p contribution represents approximately 20%. Such s-d mixing does not of course, occur for the lowest R_B state, 3"s"σ. Its calculated position (16.2 eV of 765.3 Å), agrees with the experimental value given by Fock *et al.*[6] (16.30 eV or 760.5 Å). Our calculations suggest, however, that this state would be difficult to identify unambiguously owing to its weak oscillator strength (eight times smaller than that of R_B 3"p"π) and its large width (about 70 meV or 3.2 Å).

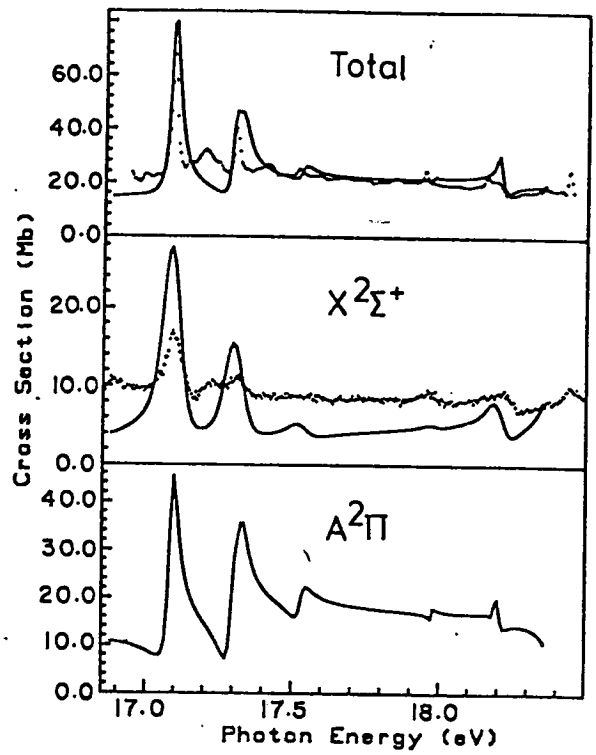

FIG. 1. Partial and total photoionization cross sections of CO in the region of the Rydberg states converging to CO^+ $B\,^2\Sigma^+$. The theoretical results are compared with the experimental data of Berkowitz (Ref. 44) (total cross section) and of Leyh *et al.* (Ref. 13) ($X\,^2\Sigma^+$ partial cross section). In order to facilitate the comparison between theory and experiment, the theoretical curves have been shifted by −0.06 eV. The calculated $X\,^2\Sigma^+$ spectrum has furthermore been broadened to a resolution of 0.05 eV (2 Å) to correspond to the experimental measurements.

B. Partial photoionization cross sections of the $X\,^2\Sigma^+$ and $A\,^2\Pi$ states

A deeper insight into the photoionization mechanisms is gained by the study of the decay channels of the Rydberg resonances, i.e., by considering the partial and vibrationally resolved cross sections. These cross sections provide useful information on the coupling between the motion of the escaping electron and the motion of the nuclei in the ion.

Our MQDT cross sections are obtained using the previously mentioned electronic quantities and vibrational overlap integrals. These integrals are introduced in the MQDT system of equations [see Eq. (18)]. The solutions of these equations are used in the calculations of the open-channel transition amplitudes [Eq. (20)] which are subsequently used in the standard expressions for the total and differential cross section (see, e.g., Starace[28] and Raoult *et al.*[19]).

Figure 1 reproduces the partial $X\,^2\Sigma^+$ and $A\,^2\Pi$ cross sections and the total ($X+A$) cross section. The energy range lies between 16.9 and 18.4 eV (730–670 Å). This purely electronic result giving resonance structures near the positions of the assignments listed in Table VI is generally in good agreement with the experiment.[45] However, part of this agreement results from a compensation of errors, the theoretical off-resonance cross section being too weak for the $X\,^2\Sigma^+$ state and too large for the $A\,^2\Pi$ state (Fig. 1). Such a situation appeared also in the work of Raoult *et al.*[19] on the isoelectronic N_2 system. Inspection of Fig. 1 shows that we also have a second peak at 17.3 and a peak at 17.59 shifted by the vibrational interval of ~0.22 eV which converges to the $Bv=1$ instead of $Bv=0$ ionic state.

The results displayed in Fig. 1 show that the most intense structures are associated with the R_B"p" (σ or π) states: such transitions are forbidden in the N_2 homonuclear case. This emphasizes the strong heteronuclear character of the CO^+ ion.

An accidental near degeneracy occurs between the R_B 3"p"π $v=1$ and 3"p"σ $v=0$ states (17.3 eV or 716.7 Å). Such a situation does not occur for the $n \geq 4$ states. In the $X\,^2\Sigma^+$ cross section the autoionization of the 3"p"π $v=1$ state was found to be dominant whereas for the A cross section the decay rates of the two near-degeneracy states are of the same order of magnitude.

The theoretical partial cross sections also show that the first members of the R_B series decay with roughly the same probability into the two open ($X\,^2\Sigma^+$ and $A\,^2\Pi$) channels, in good agreement with the photoelectron electron energy (PES) data[8,10,13] but in complete disagreement with the fluorescence electron spectroscopy (FES) results of Ito *et al.*[12] As an example, the calculated A and X branching ratios at 17.09 eV (725.5 Å) (3"p"π $v=0$ resonance) are 0.55 (X) and 0.45 (A). The PES values are[8,10,13] 0.50 (X) and 0.50 (A) whereas the FES results[12] are 0.05 (X) and 0.95 (A). No clear explanation has been found at the present time for this discrepancy. Note also that if we consider only the $A\,^2\Pi$ partial cross section, we calculate an intensity ratio of 1.10 for the two peaks 3"p"π $v=0$ and (3"p"π $v=1$) + (3"p"σ $v=0$), in agree-

ment with the experimental results of Plummer *et al.*[10] (1.0): the FES corresponding value[12] is, however, very different (1.8).

A more detailed analysis of our results shows that the R_B "p"π states decay mainly in the continua corresponding to the d and f partial waves. For the "p"σ states we found no such selectivity.

The R_B "$4s+3d$"σ resonance appears as an emission profile in the $A\,^2\Pi$ cross section. This disagrees with the experimental PES results of Plummer *et al.*[10] who observe an absorption peak in each decay channel. This discrepancy probably results from an underestimation of the corresponding interchannel interactions; this would also explain the too-weak intensity of this resonance in the X channel.

A window resonance appears in both the A and X cross sections at 18.25 eV (679.4 Å). In the X channel this structure is the emission part of the Fano profile corresponding to the R_B "$4s$-$3d$"σ state whereas, in the A cross section, it is the pure emission profile of the 3"d"π resonance. The origin of this latter profile is the strong bielectronic interaction between $B\,^2\Sigma^+$ 3"d"π which carries a very low oscillator strength and the very intense $A\,^2\Pi$ ε"d"δ channel. This behavior is exactly the same as that of the Hopfield emission series ($B\,^2\Sigma_u^+$ n"d"π_g) in N_2 which interacts strongly with the $A\,^2\Pi_u$ ε"d"δ_g channel. The emission structure at 18.87 eV (657.0 Å) (Ref. 13) in the photoionization spectrum of CO can be assigned to the next members ("$5s$-$4d$"σ,4"d"π) of the above-mentioned series.

C. Vibrationally resolved cross sections of CO^+ $X\,^2\Sigma^+$

Another important consequence of the autoionization processes concerns the vibrational selectivity with which the photoions are produced. Strong variations in the vibrational branching ratios are generally observed in the region of the autoionization resonances. As explained in Sec. II, the vibrational motion has been taken into account within the Condon approximation, i.e., neglecting the variation with R of the electronic quantities (see Sec. II B for a discussion of the consequences of this approximation). In the limit condition of an isolated Lorentzian resonance, this approximation leads to the following result[46] the part of a vibrationally resolved partial cross section which is due to a Lorentzian resonance is proportional to the product of Franck-Condon factors,

$$|\langle\chi_0|\chi_{v,\mathrm{Ryd}}\rangle|^2\,|\langle\chi_{v,\mathrm{ion}}|\chi_{v,\mathrm{Ryd}}\rangle|^2,$$

where χ_0, $\chi_{v,\mathrm{Ryd}}$, and $\chi_{v,\mathrm{ion}}$ are the vibrational wave functions which correspond to the ground and excited neutral states and to the ionic state. The vibrational branching ratios for the decay of a given vibrational level of a Rydberg member is then given by the second factor of the above expression, i.e., $|\langle\chi_{v,\mathrm{ion}}|\chi_{v,\mathrm{Ryd}}\rangle|^2$.

The vibrationally resolved partial cross sections corresponding to CO^+ $X\,^2\Sigma^+ v=0$–3 are displayed in Fig. 2 in the energy range 16.9–18.4 eV (700–670 Å). We have not introduced any vibrational structure for the $A\,^2\Pi$ state, but only considered one open electronic A channel. These theoretical results are compared with the experimental data of Leyh *et al.*[13]

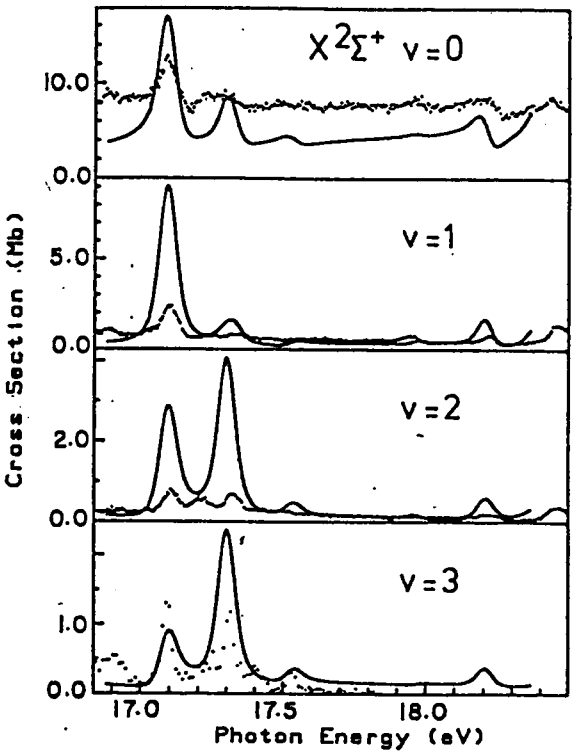

FIG. 2. Vibrationally resolved partial photoionization cross sections for the production of CO^+ $X\,^2\Sigma^+$ $v=0$–3. The experimental results are those of Ref. 13. The theoretical spectra have been broadened to a resolution of 0.05 eV and shifted by −0.06 eV.

Let us first consider the vibrational branching ratios at the energy of the 3"p"π $v=0$ resonance (17.1 eV). The MQDT values are 0.55 ($v=0$), 0.33 ($v=1$), 0.10 ($v=2$), and 0.03 ($v=3$). The $|\langle\chi_{v,\mathrm{ion}}|\chi_{v=0,\mathrm{Ryd}}\rangle|^2$ corresponding values are 0.53, 0.34, 0.10, and 0.02 whereas the experimental ratios[13] are 0.72, 0.13, 0.03, and 0.07.

At 17.30 eV (716.6 Å) the 3"p"π $v=1$ and 3"p"σ $v=0$ resonances overlap. As these resonances correspond to different symmetries, their decay channels will also have different symmetries. We can then analyze theoretically the individual branching ratios of these two resonances. For the 3"p"π $v=1$ resonance, the MQDT branching ratios are 0.36 ($v=0$), 0.03 ($v=1$), 0.39 ($v=2$), and 0.22 ($v=3$), whereas the $|\langle\chi_{v,\mathrm{ion}}|\chi_{v=1,\mathrm{Ryd}}\rangle|^2$ factors are respectively 0.31, 0.06, 0.32 and 0.22. For the 3"p"σ $v=0$ state, the MQDT branching ratios, 0.6, 0.18, 0.09 and 0.05, respectively, differ from the $|\langle\chi_{v,\mathrm{ion}}|\chi_{v=0,\mathrm{Ryd}}\rangle|^2$ factors owing to the non-negligible contribution of the background. If we do not separate the decay channels of Σ and Π symmetries, we obtain the following MQDT global branching ratios: 0.48 ($v=0$), 0.07 ($v=1$), 0.28 ($v=2$), and 0.16 ($v=3$). The corresponding experimental data are 0.74, 0.06, 0.05, and 0.09. The agreement between the theoretical and experimental results is then only qualitative.

The vibrational branching ratios depend mainly on the following quantities: the electronic transition moment for

the direct ionization (i.e., the background contribution), the electronic transition moments to the Rydberg states, the interchannel interactions, and the vibrational overlaps between the different states involved (ground states, Rydberg states, and ionic states).

Three reasons can then explain the discrepancies between the theoretical and experimental branching ratios. First of all, in the X partial cross sections, the contribution of the background is underestimated by a factor of approximately 2: this has severe consequences on the branching ratios, particularly at the energies of weak resonances. The second reason is, of course, the validity of the Condon factorization. Finally, if two nearly degenerate resonances differ in the nature of their Rydberg orbitals and in the vibrational states of their ionic cores, then the vibrational branching ratios will also depend strongly on the relative magnitude of the electronic transition moment associated with each resonance. This could partly explain the discrepancy between theory and experiment at the energy of the $3"p"\pi\ v=1$ and $3"p"\sigma\ v=0$ resonances.

With increasing vibrational number, the resonances have a tendency to assume a Lorentzian shape. This behavior is quite general when the direct transition moment to the continuum decreases as v_{ion} increases, becoming weaker and weaker with respect to the transition moment of the Rydberg state. The structure centered at 18.20 eV (681.2 Å) provides a striking example of this behavior. This structure, assigned to a superposition of the $"4s\text{-}3d"\sigma\ v=0$, $3"d"\pi\ v=0$ and $"4s+3d"\sigma\ v=1$ states, looks like a Fano profile in the $X\,^2\Sigma^+\ v=0$ cross section. The direct transition moment to the X continuum decreases rapidly with the vibrational quantum number. As a consequence, no more emission part appears in the $X\,^2\Sigma^+\ v\geq 1$ cross sections. As can be seen in Fig. 2, this behavior is correctly reproduced in our theoretical spectra. The corresponding structure, at 18.87 eV (657 Å) displays the same vibrational pattern.[13]

D. Angular distribution of the photoelectrons

The differential cross section of the ejected electrons in gas phase (with respect to ejection angle) can be expressed in terms of a simple formula in terms of total cross section, an asymmetry parameter β, and P_2 Legendre polynomial (see, e.g., Thiel[47] or Tully *et al.*[48]). Of course, the asymmetry parameter should not be confused with the channel $|i\beta)$ defined in the proceeding sections. In this section β is the asymmetry parameter only. When we look at the differential cross section at different ejection angles we speak about the angular distribution of photoelectrons. This distribution can be discussed in terms of the off- and on-resonance values of the associated β parameter. The theoretical off-resonance β value associated with the $X\,^2\Sigma^+$ state at an energy of 17 eV is 1.43 when no orthogonalization to the π^* orbital is performed. This value compares rather well with the previous theoretical values of Wallace *et al.*[49] ($\beta=1.48$) and Lucchese and McKoy[59] ($\beta=1.42$). The orthogonalization lowers β to 0.95 in reasonable agreement with the experimental value of 0.87.[51] For the $A\,^2\Pi$ state we obtain $\beta=-0.19$ at 17 eV, also in good agreement with Wallace *et al.*[49] ($\beta=-0.15$). As in the isoelectronic $N_2^+\ A\,^2\Pi_u$ case, the rapid increases of β with energy at the threshold is governed by the cosine of the difference of the Coulomb phase shifts of the $d\delta$ and $s\sigma$ dominant waves.[47] In the following we use the electronic parameters corresponding to $\varepsilon\pi$ orbitals which have been orthogonalized to the π^* antibonding orbital, as was explained in Sec. III.

When the interactions between the continua associated with different ionic cores are included, sharp variations in the cross section take place due to the presence of the Rydberg states converging to the $B\,^2\Sigma^+$ ionic state (see Fig. 3). Note that a peak in the cross section corresponds to a minimum in the β curve.

To understand this behavior we have used the partitioning scheme of Thiel.[47] In this formulation, which is based on the method of Tully *et al.*,[49] the asymmetry parameter is written as

$$\beta_i=\sum_{l}\sum_{l'}\beta_{i\,ll'}=\sum_{l,l'}\sum_{\alpha,\alpha'}\beta_{i\,ll'}^{\alpha\alpha'},$$

where i is the ionic core, l is the asymptotic channel quantum number, and α is the absolute value of the projection of the electronic angular momentum on the molecular axis.

This partitioning clearly defines the contribution to β of a given asymptotic channel l. It allows us to identify the contribution arising from each molecular symmetry, in spite of the molecule-to-laboratory-frame transformation used which mixes the molecular channels.

In Fig. 3 we also display the main diagonal and off-diagonal contributions to the β parameter for the $X\,^2\Sigma^+$ and $A\,^2\Pi$ ionic cores. In the $X\,^2\Sigma^+$ case we see that all diagonal and crossed terms involving the s, p, d, and f waves contribute to some extent to the variation of the β parameter. This interplay is particularly complicated at the positions of the R_B resonances. In the $A\,^2\Pi$ case, the situation is clearer: only the β_{A02} and β_{A22} contributions are important. The profiles induced by the R_B resonances are generally different in each $\beta_{ll'}$ curve: it is therefore very hard to analyze the effects of each resonance separately. As an example, in Table VII, we give contributions of different molecular channels to β at the maximum of the $3"p"\pi\ v=0$ resonance. We see that there is no dominant $\beta_{ll'}^{\alpha\alpha'}$ contribution to the X channel while in the A channel the $\beta_{A02}^{\sigma\delta}$ and $\beta_{A22}^{\sigma\delta}$ contributions predominate.

Figure 4 displays the variation with energy of the asymmetry parameter for each vibrational level of the X ionic core. β significantly varies between, e.g., $v=0$, 1, and 2 but shows poor agreement with the experimental data of Ederer *et al.*,[11] which only cover the region of the $3"p"\ v=0$ resonance. Also, as can be seen in Fig. 4, we calculate a depletion in the β curves corresponding to $CO^+\ X\,^2\Sigma^+$ (sum over all v_{ion} contributions) and to $CO^+\ X\,^2\Sigma^+\ v_{\text{ion}}=0$, in contrast with the experimental enhancement in both curves.

Despite this disagreement in the region of $3"p"\pi\ v=0$ resonance, our theoretical results are stable with the different calculations we have performed. Namely, in the framework of our one-configuration FCSE model, the

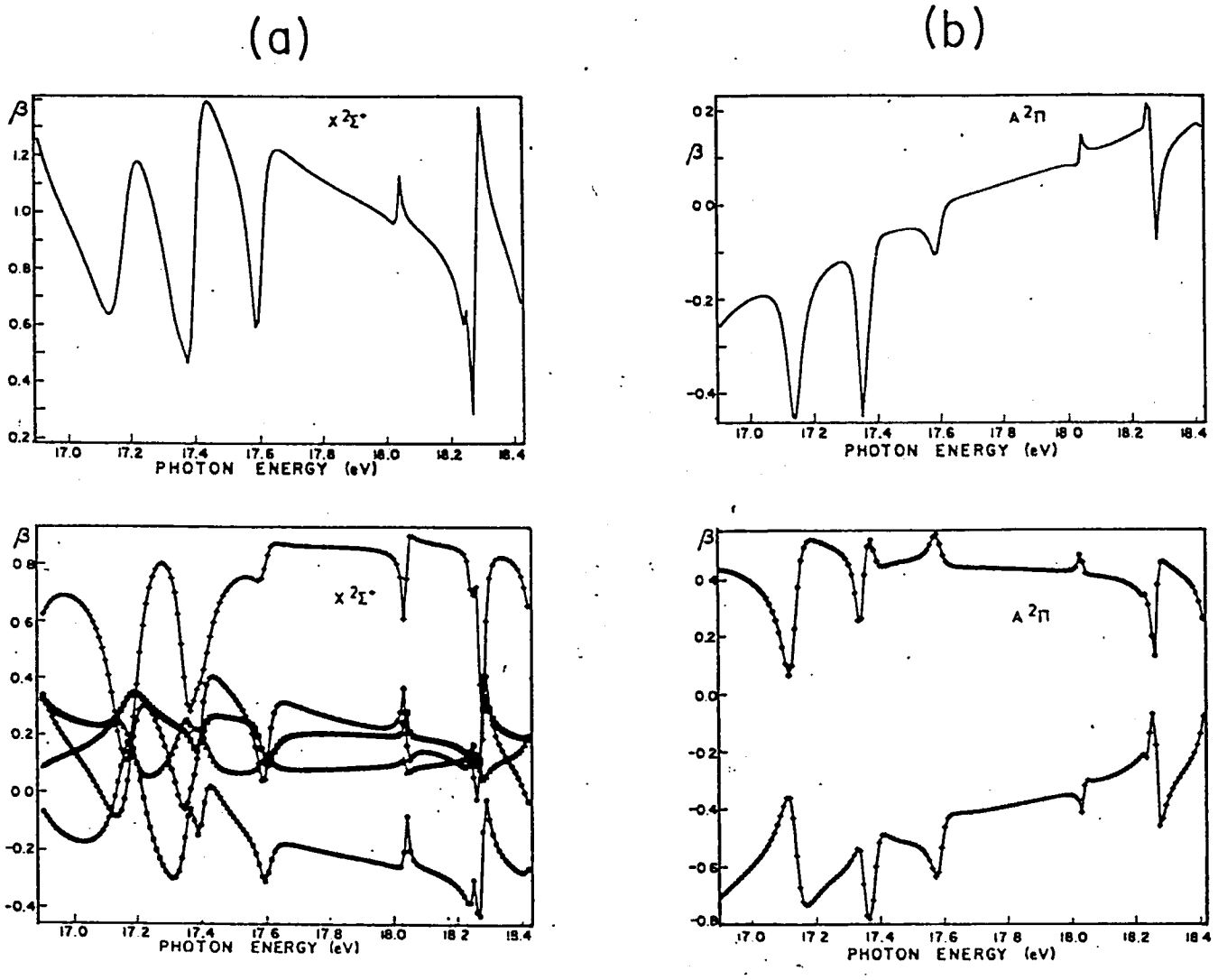

FIG. 3. Asymmetry parameter β and its decomposition in $\beta_{ll'}^{\alpha\alpha'}$ as a function of energy for (a) the $i=X\,^2\Sigma^+$ and (b) $i=A\,^2\Pi$ ionic states. In (a), the symbols $+$, $\Diamond$, $\Box$, $*$, and Δ correspond respectively to $(ll')=(11)$, (20), (22), (31), and (33). In (b), $+$ and $\Diamond$ refer to $(ll')=(20)$ and (22).

TABLE VII. Decomposition of the β parameter into its $\beta_{ll'}^{\alpha\alpha'}$ components at the maximum of the R_B $3"p"\pi$ $v=0$ resonance ($h\nu=17.147$ eV).

ll' \ $\alpha\alpha'$	$\sigma\sigma$	$\sigma\pi$	$\pi\pi$	$\beta_{ll'}$
	$X\,^2\Sigma^+$ ionic core, $\beta=0.6725$			
11	0.0276	0.0403	0.0721	0.1400
02	0.0167	−0.0905		−0.0738
22	0.0140	−0.0752	0.3378	0.2766
31	−0.0200	−0.0722	0.1727	0.0805
33	0.0031	0.0167	0.2153	0.2351

ll' \ $\alpha\alpha'$	$\sigma\sigma$	$\sigma\pi$	$\pi\pi$	$\sigma\delta$	$\pi\delta$	$\delta\delta$	$\beta_{ll'}$
	$A\,^2\Pi$ ionic core, $\beta=-0.3915$						
02	−0.1436	0.0734		−0.6046			−0.6748
22	−0.0402	0.0223	0.0071	0.3301	−0.0712	0.1208	0.3689

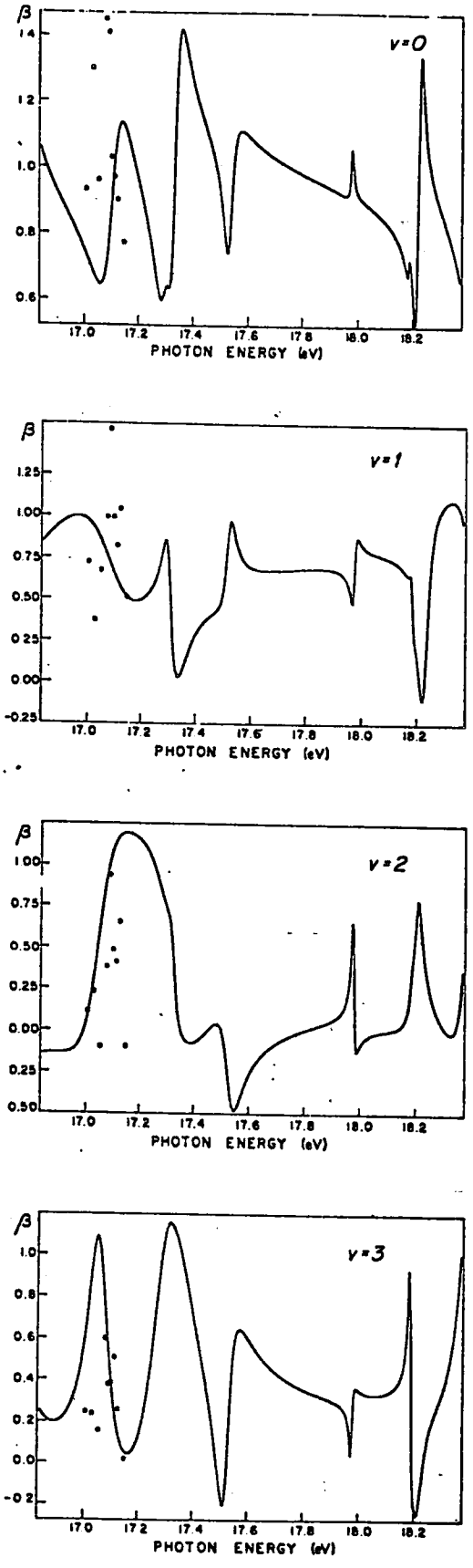

FIG. 4. Asymmetry parameter as a function of energy for the $X\,^2\Sigma^+$ $v=0$–3 levels. The experimental data are from Ederer *et al.*[11] The theoretical curves have been shifted by −0.06 eV.

electronic quantities vary smoothly as one modifies the atomic basis set or the number of terms of the multipolar expansions (see Sec. III). The same discrepancy is observed when no vibrational motion is introduced. The electronic β curves show a behavior close to the one observed in the vibrationally resolved ones. Unfortunately, the lack of detailed experimental data does not allow us to compare our calculations in a more extended region.

V. CONCLUSIONS

In this paper we have theoretically analyzed the photoionization spectrum of the CO molecule. In spite of the simple theory that we have used, the overall agreement with the experimental results is good. Particularly satisfactory agreement was found in the position and qualitative description of the resonances. These calculations have allowed us to give unambiguous assignments of the four Rydberg series converging to CO^+ $B\,^2\Sigma^+$ (see Table I). The calculated decay probabilities into the two open electronic channels $X\,^2\Sigma^+$ and $A\,^2\Pi$ are of the same order of magnitude, in agreement with all the PES results[8,10,13] but in disagreement with the FES results of Ito *et al.*[12] The satisfactory agreement between the theoretical and the experimental[13] vibrationally resolved cross sections of the $X\,^2\Sigma^+$ state shows that the Condon factorization of the electronic quantities—transition moments and interchannel interactions—provides a satisfactory framework for the interpretation of the vibrational selectivity of the electronic autoionization processes.

A comparison between the isoelectronic CO and N_2 (Ref. 19) systems in this spectral region shows that the N_2 "absorption" series corresponds to series IV in CO ("$s+d$"σ) whereas the "emission" series and the nearby shoulders correspond to the complex series III ("s-d"σ/"d"π). The intensities and quantum defects are of the same order of magnitude in the two cases. The major difference concerns the transitions to the "p"σ and "p"π series which are dipole forbidden in the N_2 case, owing to the g-u, selection rule, but give rise to the most intense structures in the CO photoionization spectrum. This strong departure from the homonuclear situation results from the large dipole moment of CO^+ $B\,^2\Sigma^+$ ($\mu=0.82$ a.u. at the center of mass) which couples the partial waves of different parities even in the asymptotic region. We must note that in the NO case (which is not isoelectronic with N_2 or CO) this latter coupling is negligible owing to the weakness of the dipole moment NO^+.

We have tried to analyze our theoretical results in terms of the leading components in the partial wave expansions. No simple picture emerges from this analysis as a strong l mixing between at least the first four partial waves (s,p,d,f) governs both the on- and off-resonance cross sections, especially for the $X\,^2\Sigma^+$ channels.

The disagreement in the angular distributions requires further work. Two weak points can be singled out in the theoretical treatment: first, the fact that the electronic quantities have been calculated at the one-configuration level; second, the use of the Condon approximation which

neglects the variation of these quantities with the internuclear distance. An easy improvement of our model would consist of the inclusion of the vibrational levels of the A ionic state. This will be discussed further below.

A few experimental structures are not reproduced in our theoretical spectra. The less-intense structures are most probably due to the R_B $v=2$ states which have not been included in our calculations. The structure located at 17.17 eV (722 Å) cannot, however, be interpreted in such a way. Ogawa and Ogawa[5] suggested that it is due to the presence of high-n Rydberg states converging to CO^+ $A\,^2\Pi$ $v=4$. These R_A states would be perturbed by the $B\,^2\Sigma^+$ $3"p"\pi$ and $3"p"\sigma$ states which could then be considered as interlopers. Such structures, called "complex resonances" have already been observed in the N_2 case by Dehmer *et al.*[52] and analyzed in detail by Guister-Suzor and Lefebvre-Brion.[53] In order to check the assignment of Ogawa and Ogawa,[5] we have performed detailed calculations in the 17—17.4-eV region by explicitly introducing the vibrational channels in the $A\,^2\Pi$ core with their respective thresholds. These results will be presented in a forthcoming paper.

ACKNOWLEDGMENTS

We are indebted to Hélène Lefebvre-Brion for stimulating discussions, participation in the initial stages of the work, and for a critical reading of the manuscript. We are grateful to Annick Giusti-Suzor and Stephen C. Ross for critically reading the manuscript. Thanks are due to Hervé Le Rouzo for providing us with a tricenter version of an integral program written by Schaefer III. We thank P. Bagus, M. Yoshimine, and B. Liu for providing us with a version of the Alchemy system of programs. We are grateful to Dr. Ederer, Dr. Parr, Dr. Cole, Dr. Stockbauer, and Dr. Dehmer for providing us with numerical points of their published data.[11] B.L. acknowledges discussions with J. Delwiche and M. J. Hubin-Franskin. The authors are grateful to the North Atlantic Treaty Organization (NATO) Contract No. 096.82, to the Belgian Government (Action de Recherche Concertée), and to the Fonds de La Recherche Fondamentale Collective (Belgium) for their financial support. B. L. thanks the Fonds National de la Recherche Scientifique (Belgium) for support.

[1]Y. Tanaka, Sci. Papers Inst. Phys. Chem. Res. (Tokyo) 39, 447 (1942).
[2]H. J. Henning, Ann. Phys. (N.Y.) 13, 599 (1932).
[3]R. E. Huffmann, J. C. Larrabee, and Y. Tanaka, J. Chem. Phys. 40, 2261 (1964).
[4]M. Ogawa, J. Chem. Phys. 43, 2142 (1965).
[5]M. Ogawa and S. Ogawa, J. Mol. Spectrosc. 41, 393 (1972).
[6]J. H. Fock, P. Gürtler, and E. E. Koch, Chem. Phys. 47, 87 (1980).
[7]E. Lindholm, Ark. Fys. 40, 103 (1969).
[8]J. A. R. Samson and J. L. Gardner, J. Electron Spectrosc. Relat. Phenom. 8, 35 (1976).
[9]J. L. Gardner and J. A. R. Samson, J. Electron Spectrosc. Relat. Phenom. 13, 7 (1978).
[10]E. W. Plummer, T. Gustaffson, W. Gudat, and D. E. Eastman, Phys. Rev. A 15, 2339 (1977).
[11]D. L. Ederer, A. C. Parr, B. E. Cole, R. Stockbauer, J. L. Dehmer, J. B. West, and K. Codling, Proc. R. Soc. London Ser. A 378, 423 (1981).
[12]K. Ito, A. Tabché-Fouchailé, H. Fröhlich, P. M. Guyon, and I. Nenner, J. Chem. Phys. 82, 1231 (1985).
[13]B. Leyh, M.-J. Hubin-Franskin, J. Delwiche, and I. Nenner (unpublished).
[14]T. Betts and V. McKoy, J. Chem. Phys. 54, 113 (1971).
[15]Ch. Jungen, J. Chem. Phys. 53, 4168 (1970).
[16]A. Guisti-Suzor and H. Lefebvre-Brion, Chem. Phys. Lett. 76, 132 (1980).
[17]A. Guisti-Suzor and Ch. Jungen, J. Chem. Phys. 80, 986 (1984).
[18]P. Morin, I. Nenner, M. Y. Adam, M.-J. Hubin-Franskin, J. Delwiche, H. Lefebvre-Brion, and A. Guisti-Suzor, Chem. Phys. Lett. 92, 609 (1982).
[19]M. Raoult, H. Le Rouzo, G. Raşeev, and H. Lefebvre-Brion, J. Phys. B 16, 4601 (1983).
[20]G. Raşeev, J. Phys. B 18, 423 (1985).
[21]L. A. Collins and B. I. Schneider, Phys. Rev. A 29, 1695 (1984).
[22]H. Le Rouzo and G. Raşeev, Phys. Rev. A 29, 1214 (1984).
[23]H. Feshbach, Ann. Phys. (N.Y.) 5, 357 (1958).
[24]H. Feshbach, Ann. Phys. (N.Y.) 19, 287 (1962).
[25]W. Domcke, Phys. Rev. A 28, 2777 (1983).
[26]L. S. Rodberg and R. M. Thaler, *Introduction to the Quantum Theory of Scattering* (Academic, New York, 1967), p. 77.
[27]A. Giusti-Suzor and U. Fano, J. Phys. B 17, 4267 (1984).
[28]A. F. Starace, *Theory of Atomic Photoionization*, Vol. 31 of *Handuch der Physik*, edited by S. Flügge (Springer-Verlag, Berlin, 1982).
[29]G. Raşeev, H. Le Rouzo, and H. Lefebvre-Brion, J. Chem. Phys. 72, 5701 (1980).
[30]G. Raşeev, Comput. Phys. Commun. 20, 267,275 (1980).
[31]H. Lefebvre-Brion, J. Mol. Spectrosc. 19, 103 (1973).
[32]C. Greene and Ch. Jungen, *Advances in Atomic and Molecular Physics* (Academic, New York, 1985), Vol. 21, p. 51.
[33]U. Fano, Phys. Rev. A 2, 353 (1970).
[34]Ch. Jungen and D. Dill, J. Chem. Phys. 73, 3338 (1980).
[35]Ch. Jungen and O. Atabek, J. Chem. Phys. 66, 5584 (1977).
[36]U. Fano and D. Dill, Phys. Rev. A 6, 185 (1972).
[37]D. Dill and J. L. Dehmer, J. Chem. Pgys. 61, 692 (1974).
[38]W. M. Huo, J. Chem. Phys. 45, 1554 (1966).
[39]A. D. McLean and M. Yoshimine, *Tables of Linear Molecule Wave Functions* [IBM J. Res. Dev., Suppl. 12, 206 (1968)].
[40]M. A. Morrisson and L. A. Collins, J. Phys. B 10, L119 (1977).
[41]R. R. Lucchese, G. Raşeev, and V. McKoy, Phys. Rev. A 25, 2572 (1982) and references therein.
[42]H. Le Rouzo (unpublished).
[43]K. P. Huber and G. Herzberg, *Constants of Diatomic Molecules* (Van Nostrand Reinhold, New York, 1979).
[44]P. Felenbok, Ann. Astrophys. 26, 393 (1963).
[45]J. Berkowitz, *Photoabsorption, Photoionization and Photoelectron Spectroscopy* (Academic, New York, 1979), p. 228.
[46]A. L. Smith, Philos. Trans. R. Soc. London, Ser A 268, 169 (1970).
[47]W. Thiel, Chem. Phys. Lett. 87, 249 (1982); Chem. Phys. 77,

103 (1983).
[48]J. C. Tully, R. S. Berry, and B. J. Dalton, Phys. Rev. 176, 95 (1968).
[49]S. Wallace, D. Dill, and J. L. Dehmer, J. Phys. B 12, L417 (1979).
[50]R. R. Lucchese and V. McKoy, Phys. Rev. A 28, 1382 (1983).
[51]G. V. Marr, J. M. Morton, R. M. Holmes, and D. G. McCoy, J. Phys. B 12, 43 (1979).
[52]P. M. Dehmer, P. J. Miller, and W. A. Chupka, J. Chem. Phys. 80, 1030 (1984).
[53]A. Giusti-Suzor and H. Lefebvre-Brion, Phys. Rev. A 30, 3057 (1984).